MULTIPERIODICITY, CHAOS, AND INTERMITTENCY IN A REDUCED MODEL OF THE SOLAR CYCLE

PAUL CHARBONNEAU
High Altitude Observatory, National Center for Atmospheric Research, P.O. Box 3000, Boulder, CO 80307-3000, U.S.A.

(Received 23 October 2000; accepted 6 December 2000)

Abstract. In a recent paper, Durney (2000) has discussed a physically plausible procedure whereby the dynamo equations describing magnetic field regeneration in Babcock–Leighton models of the solar cycle can be reduced to a one-dimensional iterative map. This procedure is used here to investigate the behavior of various dynamo-inspired maps. Durney's explanation of the so-called odd–even effect in sunspot cycle peak amplitudes, which he ascribed to a period-2 limit cycle, is found to be robust with respect the choice of nonlinearity defining the map, and to the action of strong stochastic forcing. In fact, even maps without limit cycles are found to show a strong odd–even signal in the presence of forcing. Some of the stochastically forced maps are found to exhibit a form of on-off intermittency, with periods of activity separated by quiescent phases of low cycle amplitudes. In one such map, a strong odd–even signal is found to be a good precursor to the transition from bursting to quiescent behavior.

1. Introduction: the Fluctuating Solar Cycle

Already in his 1843 landmark paper announcing the discovery of the sunspot cycle, S.H. Schwabe provided evidence for a variation in its peak amplitude. Later observations and historical analysis of earlier observations (see, e.g., Hoyt and Schatten, 1998) have amply demonstrated that both the amplitude and duration of sunspot cycles can vary significantly from one cycle to the next. In itself this is not terribly surprising, given that the dynamo process responsible for the underlying regeneration of the solar magnetic field most certainly involves interactions between the magnetic field and the turbulent convective fluid motions pervading the solar convective envelope.

With sunspot numbers taken as a proxy of the underlying magnetic cycle, the solar cycle nonetheless exhibits significant patterns that betray some order behind the observed fluctuations. One such regularity is the well-documented anti-correlation existing between the cycle amplitude and duration (e.g., Hoyng, 1993, Section 7; Ossendrijver, Hoyng, and Schmitt, 1996; Charbonneau and Dikpati, 2000; Figure 1). Another is the so-called odd–even effect, which refers to statistically significant systematic correlations between various properties of sunspot cycle triads $(n, n+1, n+2)$, where n is the cycle number. The odd–even effect has been of

Solar Physics **199:** 385–404, 2001.

interest because of its potential for prediction of solar-cycle amplitudes (see, e.g., Wilson, 1988).

Figure 1 illustrates the odd–even effect as observed in the sunspot record. The peak amplitude A_n of sunspot cycles 1–22 (Figure 1(A), solid dots) is calculated from the smoothed monthly sunspot number time series available from the Solar Index Data Center (Brussels), and plotted against cycle number. Odd- (even-) numbered cycle amplitudes have been joined by dashed (dotted) line segments. The thick solid line is a running mean $\langle A_n \rangle$ computed using a 1–2–1 averaging filter:

$$\langle A_n \rangle = \tfrac{1}{4}(A_{n-1} + 2A_n + A_{n+1}) \; . \tag{1}$$

The odd–even effect in peak amplitude shows up most clearly by using the running mean so calculated to detrend the raw amplitude sequence. This is carried out on Figure 1(B), showing now the sequence $A_n - \langle A_n \rangle$ as a function of cycle number. This detrended format is used repeatedly in what follows. From cycles 9 to 21, odd-numbered cycles have systematically higher-than-average amplitudes than even-numbered cycles.

In a recent paper, Durney (2000) has presented a clever procedure whereby simplified forms of the partial differential equations governing magnetic field regeneration in Babcock–Leighton dynamos can be reduced to a one-dimensional map, i.e., an iteration algorithm having the general form

$$A_{n+1} = g(A_n) \; , \qquad n = 0, 1, 2, \ldots \; , \tag{2}$$

thus expressing the amplitude of sunspot cycle n as a (nonlinear) function of the amplitude of the preceding cycle. Durney's procedure is reviewed in Section 2, together with a second physically-inspired variation, and the behavior of the resulting maps is examined in some details. Section 3 focuses on the effect of stochastic forcing on the two maps introduced in Section 2, with particular focus on the robustness of the odd–even effect, and the emergence of intermittency for stochastically forced maps in the presence of low-amplitude additive noise. Section 4 is a comparative case study, wherein the amplitude fluctuations characterizing a recently published simulation of a stochastically forced Babcock–Leighton solar cycle model (Charbonneau and Dikpati, 2000) is compared and contrasted to the behavior seen in amplitude iterates computed via an equivalent map. The paper concludes (Section 5) with a critical discussion of the physical correspondence between the behavior of the one-dimensional maps studied here, and the real solar cycle.

2. Reduction of the Dynamo Equations to a Map

Only a brief outline of Durney's procedure is given here, with the interested reader being referred to Durney (2000) for full details. Like dynamo models based on

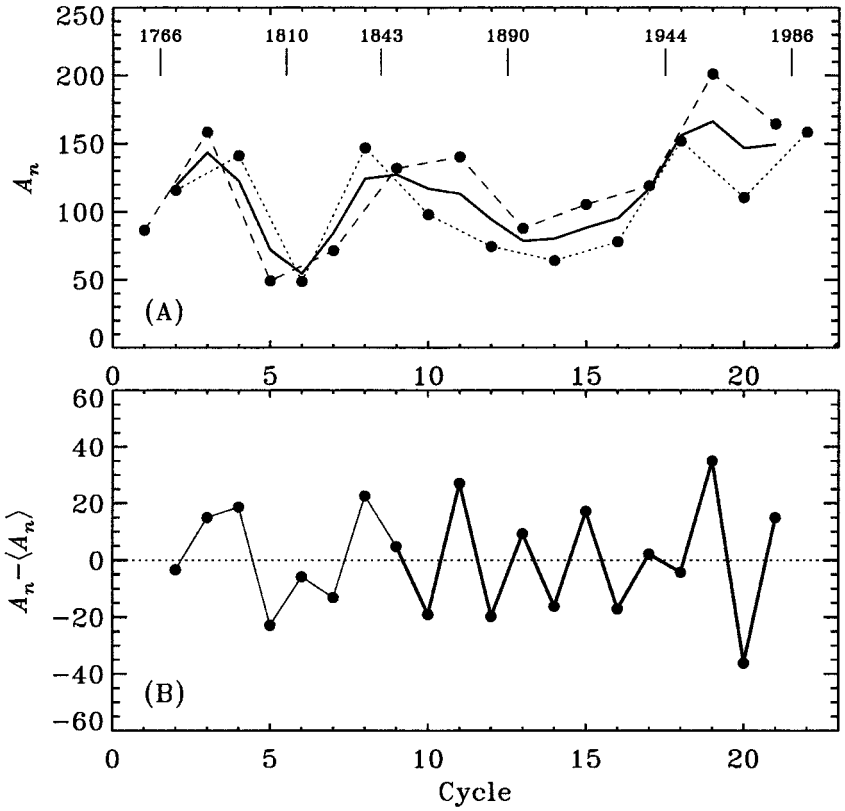

Figure 1. The odd–even effect in sunspot data. (A) shows the peak amplitude A_n of successive sunspot cycles (*solid dots*), inferred from the smoothed monthly sunspot numbers (13-month running mean) from the SIDC. The *dashed* (*dotted*) *line* segments connect the odd-numbered (even-numbered) cycles, and the *thick solid line* is a running mean $\langle A_n \rangle$ based on $1-2-1$ averaging filter (see Equation (1)). (B) shows the detrended time series obtained by subtracting the running mean $\langle A_n \rangle$ from the A_n time series. The odd–even effect shows up quite clearly and remains uninterrupted from cycle 9 to 21.

mean-field electrodynamics, Babcock–Leighton dynamos rely on the shear of a large-scale poloidal field by differential rotation to produce a toroidal magnetic component. They differ from mean-field models in invoking the decay of bipolar active regions showing a net tilt with respect to the east-west direction to regenerate the poloidal magnetic field (see, e.g., Durney, 1997; Dikpati and Charbonneau, 1999; Nandy and Choudhuri, 2000, and references therein).

2.1. DURNEY'S REDUCTION PROCEDURE

The starting point of the Durney (2000) reduction procedure is the realization that in Babcock–Leighton models, the production of the toroidal magnetic field T_{n+1}

at cycle $n+1$ in the shear layer at the core–envelope interface is proportional to the surface poloidal magnetic field P_n of the *preceding* cycle:

$$T_{n+1} = (\Delta\Omega)(\Delta t) P_n \, . \tag{3}$$

Equation (3) is pre-empted on the assumption that the poloidal field experiences neither growth nor decay during the time interval Δt ($= (L - L_2)u^{-1}$ in the notation of Durney (2000)) required to be advected by meridional circulation from the surface down to the equatorial part of the shear layer, and that during this time the poloidal field is being acted upon by a constant rotational shear $\Delta\Omega$. In keeping with the Babcock–Leighton picture, the production of the poloidal field is assumed to be a function of the toroidal field of the current cycle, in some proportion to the amplitude of the toroidal field:

$$P_{n+1} = f(T_{n+1}) T_{n+1} \, , \tag{4}$$

where $f(T_{n+1})$ is an as-yet unspecified function measuring the efficiency of the Babcock–Leighton mechanism as a function of the toroidal field strength in the shear layer (more on this below). Let now $\bar{P}$, $\bar{T}$ be representative values for the poloidal and toroidal field amplitudes, and convert Equations (3) and (4) to non-dimensional form:

$$t_{n+1} = a p_n \, , \tag{5}$$

$$p_{n+1} = (\bar{T}/\bar{P}) f(t_{n+1}) t_{n+1} \, , \tag{6}$$

where $p_n = P_n/\bar{P}$, $t_n = T_n/\bar{T}$, and $a = (\bar{P}/\bar{T})\Delta\Omega\Delta t$. This latter dimensionless parameter can be set to $a = 1$ without loss of generality, since it can be readily absorbed in the upcoming definition of $f(t_{n+1})$. Substituting Equation (5) into Equation (6) then yields

$$p_{n+1} = (\bar{T}/\bar{P}) f(p_n) p_n \, . \tag{7}$$

Durney (2000) chooses

$$f(t_{n+1}; \beta) = (\bar{P}/\bar{T})(1 + \beta(1 - t_{n+1})) \, , \quad \beta > 0 \, , \tag{8}$$

where the parameter β effectively measures the efficiency of the Babcock–Leighton mechanism of poloidal field regeneration*. Inserting Equation (8) into (7) immediately leads to

$$p_{n+1} = p_n(1 + \beta(1 - p_n)) \, , \quad [\, \equiv g(p_n; \beta) \,] \, , \quad \beta > 0 \, , \tag{9}$$

* It will become clearer in in Section 4 below that the map's parameter, here β, plays the role of a dynamo number.

i.e., a one-dimensional parametric iterative map (hereafter 'map', for brevity). Durney (2000) then goes on to show that for $2 \lesssim \beta \lesssim 2.45$, Equation (9) yields a sequence of amplitude iterates p_n's alternating between higher- and lower-than-average, in a manner reminiscent of the odd–even effect observed in sunspot data.

2.2. MULTIPERIODICITY AND CHAOS IN ONE-DIMENSIONAL MAPS

Equation (9) is one of many variations on the so-called logistic map $p_{n+1} = \alpha p_n(1 - p_n)$, which has been studied in great detail in the context of ecological population dynamics (see, e.g., Holton and May, 1993), and since the work of Feigenbaum (1978) has become an icon of deterministic chaos in low-dimensional dynamical systems. Figure 2 shows four sequences of p_n iterates generated from Equation (9), with increasing values of β from top to bottom. The first sequence ($\beta = 1.9$) is characterized by a fixed amplitude $p_n = 1$ as the map is iterated, a behavior that characterizes the parameter range $0 \leq \beta \leq 2.0$. The second sequence ($\beta = 2.3$) shows the behavior emphasized by Durney (2000), and holds in the range $2.0 \leq \beta \leq 2.4494$. Further increase of β leads to more complex cyclic behavior (third sequence, $\beta = 2.5$), until all appearance of regularity is lost (fourth sequence, $\beta = 2.7$).

A solution of the form $p_{n+1} = p_n$ is a *fixed point* (denoted μ) of the map. Examination of Equation (9) immediately shows that the trivial solution $p_n = 0$ as well as $p_n = 1$ are both fixed points, independently of the assumed value of β. However, for this map the trivial solution $p_n = 0$ has a basin of attraction of zero measure, i.e., it is accessible only with $p_0 = 0$ and under exact arithmetics. The other fixed point $\mu = 1$ is an *attractor* of the system up to $\beta = 2$, where it loses stability to a period-2 limit cycle, i.e., a solution of the form $p_{n+2} = p_n$. This loss of stability is a well-understood process in the context of iterative maps (see, e.g., Holton and May, 1993, Section 5.3.2), and occurs at the value of β such that

$$\left.\frac{\mathrm{d}g(p_n;\beta)}{\mathrm{d}p_n}\right|_{p_n=\mu} \leq -1\,. \tag{10}$$

Similarly, the period-2 limit cycle eventually loses stability to a period-4 limit cycle (third sequence on Figure 2), which later becomes unstable to a period-8 limit cycle, and so on.

The varying behavior of the iterates is best viewed by plotting successive values of p_n against β, after disappearance of any transient associated with the choice of p_0. Figure 3(A) shows one such bifurcation diagram, for the map defined by Equation (9) above. The various branches represent stable solutions, in that the p_n iterates always return to those stable values following external perturbation (cf., Figure 2, dotted and solid lines for the upper three sequences). Examination of the bifurcation diagram also reveals that something peculiar seems to be happening beyond $\beta \gtrsim 2.57$. Successive iterates fill an ever-widening p_n range, and this time small external perturbations are amplified exponentially as the iteration proceeds

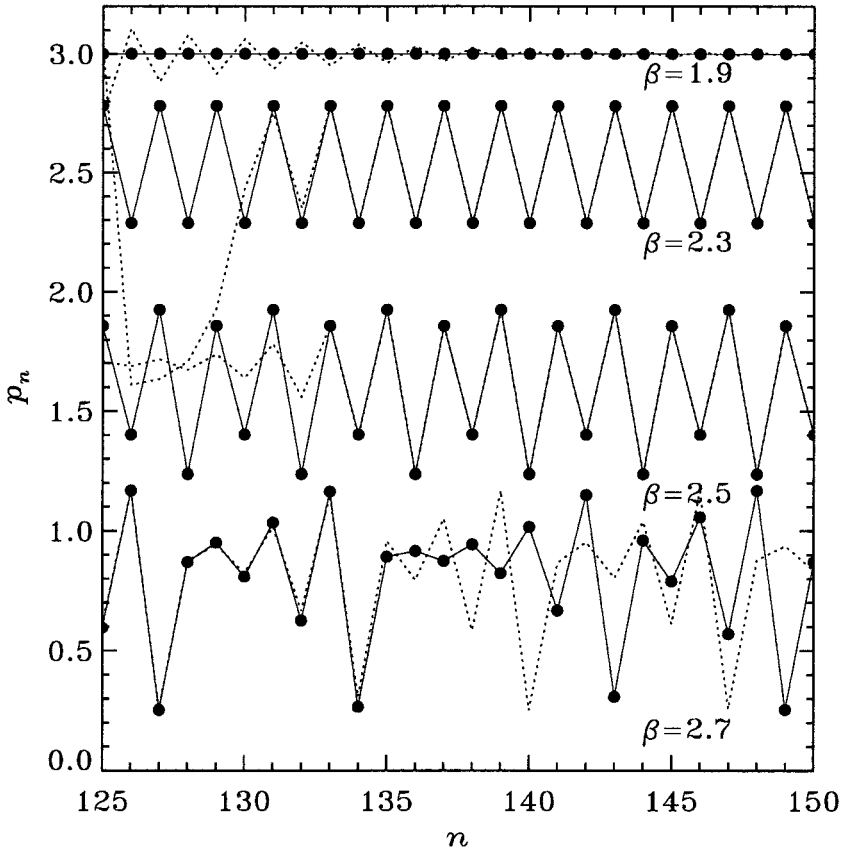

Figure 2. Four sequences of iterates p_n obtained with Equation (9) for four different values of the control parameter β, as indicated. The *dotted lines* indicate the fate of perturbed solutions. For the first three sequences, a strongly perturbed p_{125} returns to its stable limit cycle within a few tens of iterations. In contrast, for $\beta = 2.7$ (*bottom sequence*) a 1% perturbation imposed at iteration 125 is exponentially amplified, a classical indicator of chaotic behavior.

(cf., solid and dotted lines on fourth sequence on Figure 2). For $\beta \gtrsim 2.57$, Equation (9) exhibits *chaotic behavior*. Finally, for $\beta \geq 3.0$ the map is unstable, i.e., the iterate sequence diverges to $\pm\infty$.

Feigenbaum (1978) has demonstrated a truly unique aspect of the bifurcation diagram shown on Figure (3): it is *universal* to one-dimensional maps characterized by a single critical point, i.e., maps $g(p_n)$ for which $\mathrm{d}g/\mathrm{d}p_n = 0$ for one and only one p_n in the map's range (also called 'single-hump' maps). Whatever the functional form of $g(p_n)$, the transition to chaos always proceeds through the same geometric sequence of bifurcations through period-2^m limit cycles, with $m = 0, 1, 2, \ldots$

Let the β values at which the map undergoes successive bifurcations be denoted $\lambda_1, \lambda_2, \lambda_3 \ldots$, etc. Feigenbaum (1978) showed that, for all sufficiently steep one-

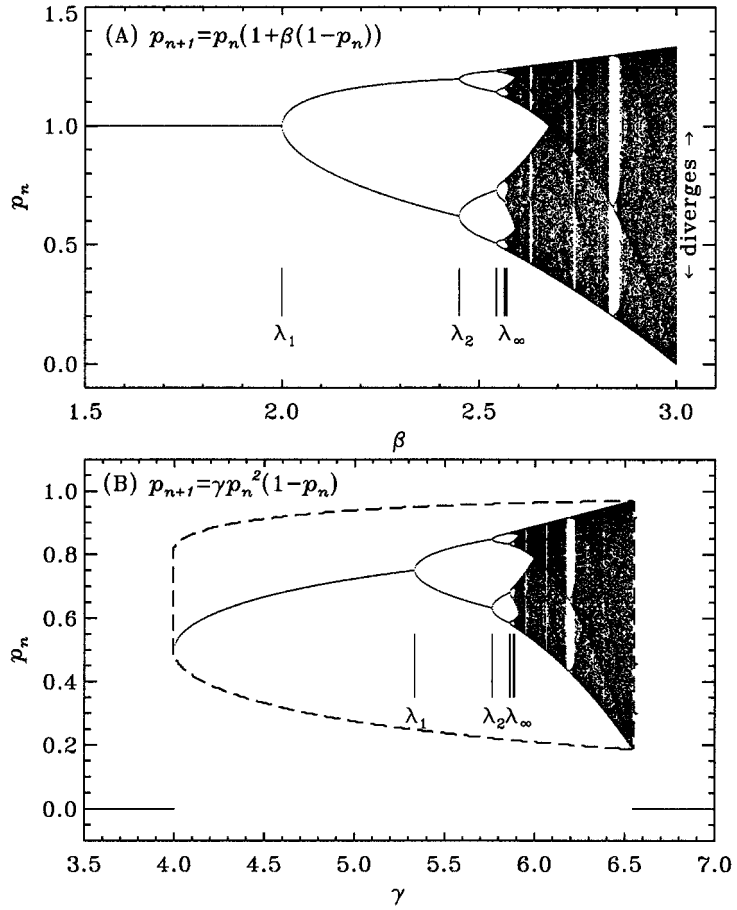

Figure 3. (A) is a bifurcation diagram for the one-dimensional map defined by Equation (9). The vertical line segments indicate the values of $\beta = \lambda_m$ at which the first few bifurcations occur, as well as the value $\beta \to \lambda_\infty = 2.5699$ at which transition to chaos takes place. For $\beta > 3$ the sequence of iterates diverges to $\pm\infty$. (B) is a similar bifurcation diagram for the alternate map defined by Equation (13). Note that non-trivial behavior is now restricted to the range $4.0000 \leq \gamma \leq 6.5433$, outside of which the only stable state is $p_n = 0$. Moreover, even within this range the trivial solution $p_n = 0$ still retains a basin of attraction of finite measure, corresponding to the area located outside the closed dashed contour in (B). The transition to chaos now takes place at $\gamma = 5.8878$. The two bifurcation diagrams are otherwise topologically identical, as expected from the universal character of single-hump one-dimensional maps (see text).

dimensional single-hump maps (i.e., maps that satisfy Equation (10) at some value of the map's parameter)

$$\lim_{m\to\infty} \frac{\lambda_{m-1} - \lambda_m}{\lambda_m - \lambda_{m+1}} = \delta = 4.669201\ldots, \tag{11}$$

where the universal constant δ is since known as Feigenbaum's number. One great practical advantage of Equation (11) is that it provides a recurrence relation allow-

ing one to calculate the value λ_∞ at which transition to chaos takes place, from measurement of the first few bifurcation points. This yields $\lambda_\infty = 2.5699\ldots$ for the bifurcation diagram plotted in Figure 3(A). The reader further interested in the behavior of one-dimensional maps should consult the very lucid and accessible introduction provided by Holton and May (1993).

2.3. An alternate map

Given the universal character of single-hump maps, one might ask whether there exist other choices for $f(t_{n+1})$ in Equation (6) that would represent a better approximation to the physics of the Babcock–Leighton mechanism. Equation (8), adopted by Durney (2000), expresses the fact that the efficiency of poloidal field production decreases as the toroidal field increases in strength. This is indeed borne out by the simulations of rising thin flux tubes, which have shown that for toroidal field strengths in excess of about 100 kG, flux ropes emerge parallel to the E–W direction (see, e.g., D'Silva and Choudhuri, 1993; Caligari, Moreno-Insertis, and Schüssler, 1995), i.e., without the tilt that is essential to the Babcock–Leighton mechanism. However, such simulations have also shown that for toroidal field strengths below about 10 kG the flux ropes emerge at high latitudes and with tilt patterns incompatible with Joy's Law. Moreover, such weak flux ropes are easily randomized by stochastic buffeting associated with the turbulent fluid motions in the convective envelope (Longcope and Fisher, 1996). Perhaps even more important, simulations indicate that these weak flux ropes do not even survive their rise through the convective envelope, 'exploding' on their way up due to excess buoyancy (Moreno-Insertis, Caligari and Schüssler, 1995). This implies that the Babcock–Leighton mechanism is characterized by both lower and upper operating thresholds. It also suggests that poloidal field production decreases faster than t_n as the toroidal field falls below 10 kG or so. A simple alternate form of Equation (8) capturing this latter behavior is

$$f(t_{n+1};\gamma) = (\bar{P}/\bar{T})\gamma\, t_{n+1}(1 - t_{n+1})\,, \quad \gamma > 0\,, \tag{12}$$

so that Equation (7) now becomes

$$p_{n+1} = \gamma\, p_n^2(1 - p_n)\,, \quad [\ \equiv g(p_n;\gamma)\ ]\,, \quad \gamma > 0\,. \tag{13}$$

The corresponding bifurcation diagram is shown in Figure 3(B). It is topologically equivalent to that plotted in Figure 3(A), as expected from Feigenbaum's universality result, with two important differences. First, non-trivial behavior (i.e., $\lim_{n\to\infty} p_n \neq 0$) is restricted to the parameter range $4.0 < \beta < 6.5433$. Outside of this range any initial p_0 rapidly decays to zero. In addition, even within this range the attractor has a bounded basin of attraction, indicated by the dashed closed contour in Figure 3(B). Any iterate sequence starting with a value p_0 located outside this closed region converges to $p_n = 0$. This has some interesting consequences, to

be explored further below. In contrast, there is no such finite size basin of attraction to the trivial solution for the map defined by Equation (9).

For the map defined by Equation (13), the 2-cycle odd–even effect materializes in the interval $16/3 \leq \gamma \leq 5.7635$, and transition to chaos takes place as $\gamma \rightarrow \lambda_\infty = 5.8878$. Figure 3 thus demonstrates that the explanation of the odd–even effect for sunspot number data, as put forth by Durney (2000), does not depend sensitively on the choice of the amplitude-limiting function $f(t_{n+1})$.

3. Stochastically Forced Maps

Whatever one might think of the reduction of the dynamo process to a one-dimensional map, it is clear that the resulting explanation for the odd–even effect is predicated on a (relatively) fine tuning of some control parameter ($2.0 \leq \beta \leq 2.4494$ in Equation (9), $16/3 \leq \gamma \leq 5.7635$ in Equation (13)). This would suggest that this explanation for the sunspot cycle's odd–even effect is not particularly robust; given that the dynamo operates at least in part in the turbulent convective envelope, the parameter β (or γ) might be expected to vary stochastically over a significant range of numerical values, possibly taking the dynamo outside the range in γ where the 2-cycle behavior holds. To test this possibility, consider now a stochastically forced version of Equation (13), defined as follows:

$$p_{n+1} = \gamma_n p_n^2 (1 - p_n) + \varepsilon_n \,, \tag{14}$$

where the map's parameter γ_n is now drawn anew at each iteration from a sequence of random deviate uniformly distributed in some preset interval $[\gamma_1, \gamma_2]$. Similarly, ε_n is drawn from a separate sequence of random deviate distributed in $[0, \varepsilon]$, with $\varepsilon \ll 1$. This formulation thus implies that the map is subjected to both multiplicative and additive noise, the latter of low amplitude.

3.1. Persistence of the odd–even effect

Figure 4 shows a short portion of the amplitude iterate sequence generated from Equation (14), with $\gamma_n \in [4.5, 6.5]$ and $\varepsilon_n \in [0, 0.09]$. The overall format is similar to Figure 1 above: (A) is the amplitude sequence p_n, with the thick solid line corresponding to a 1–2–1 running mean $\langle p_n \rangle$ (see Equation (1)). (B) is the detrended sequence $p_n - \langle p_n \rangle$. Note the clear odd–even pattern persisting from iteration 551 to 566, with the pattern also present for other shorter iteration intervals (emphasized by thicker line segments).

It might appear surprising that the odd–even effect still shows up so clearly, given that the imposed range $\gamma_n \in [4.5, 6.5]$ implies that γ_n lies outside the interval $[\lambda_1, \lambda_2]$ for about 88% of iterations. The reason lies with the fact that, at fixed γ, the convergence to the corresponding fixed point or limit cycle is often oscillatory, so that the fluctuating map responds in an 'overstable' manner to the stochastically

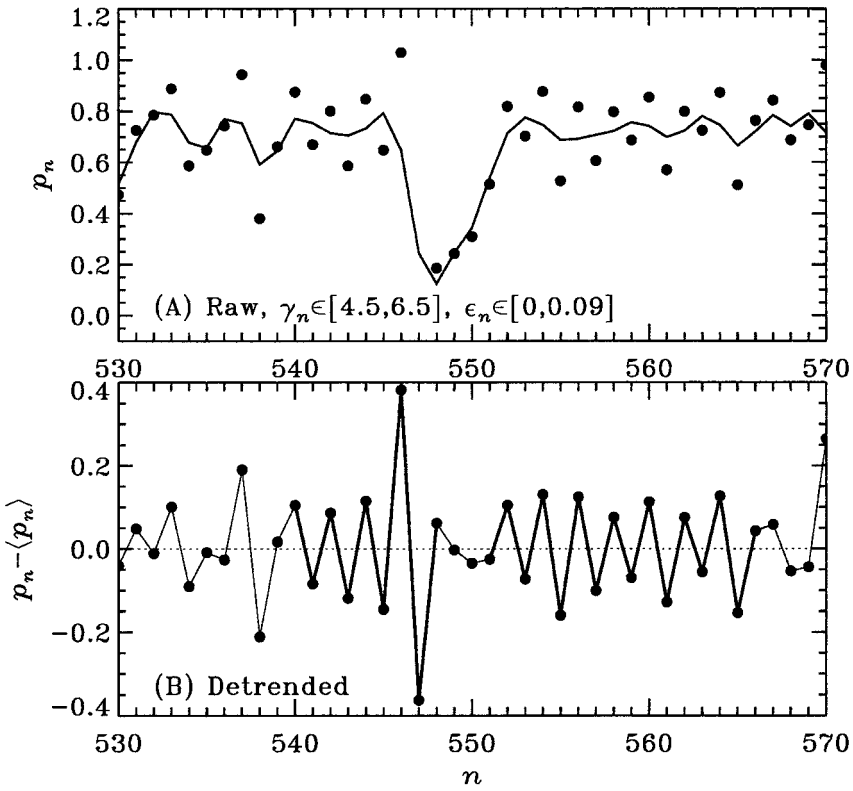

Figure 4. Portion of an amplitude iterate sequence for a stochastically forced version of Equation (13), with $\gamma \in [4.5, 6.5]$. (A) is the raw iterate sequence, with the *thick line* corresponding to a 1–2–1 running mean, while (B) is the detrended sequence. Notice the persistence of the odd–even effect from iteration 540 to 547 and 551 to 566.

varying γ_n (see, e.g., dotted lines in Figure 2). The same behavior is obtained with a stochastically forced version of Equation (9), the original map proposed by Durney (2000).

3.2. INTERMITTENCY

There are additional effects of stochastic forcing that require a look at a longer sequence of amplitude iterates. Figure 5 shows a 2000 iteration sequence, for the same parameter settings as the sequence plotted in Figure 4(A), with the latter corresponding to the dotted box. The sequence is exhibiting *intermittency*, i.e., it alternates between quiescent phases with $p_n \sim \varepsilon$, and bursting phases with $p_n \sim 1$. A similar behavior has been observed before with a stochastically-driven one-dimensional logistic maps by Heagy, Platt, and Hammel (1994), who identify it with the so-called on-off intermittency studied by Platt, Spiegel, and Tresser (1993). On-off intermittency occurs when one dynamical variable – here the stochastically fluctuating γ_n – pushes the system across a transcritical bifurcation

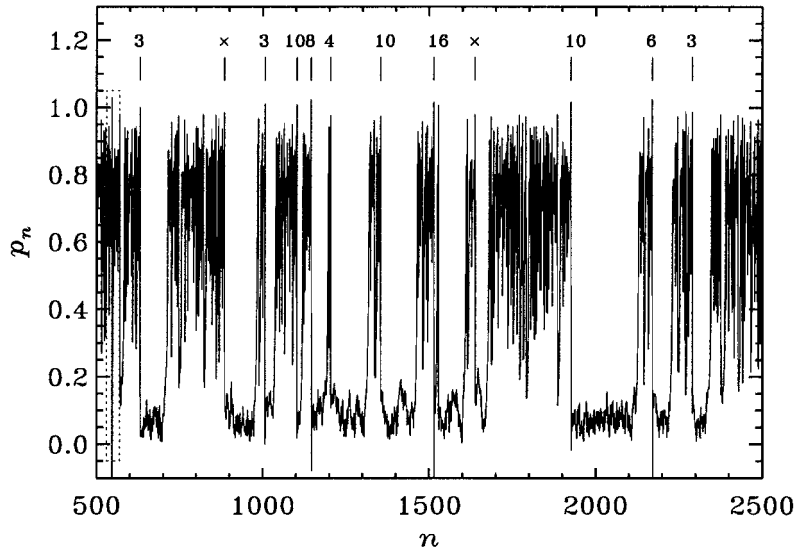

Figure 5. A much longer sequence of amplitude iterates p_n for the stochastically forced Equation (14) with $\gamma \in [4.5, 6.5]$ and $\varepsilon_n \in [0, 0.09]$. The *dotted box* indicates the portion of the sequence plotted in Figure 4. The vertical tick marks along the upper horizontal axis flag the termination of the bursting phases, and are labeled according to the number of preceding iterations during which a clear odd–even signal is present. A '×' indicates that no such effect was seen for more than 3 preceding iterations, which is taken to be the minimum required to define an odd–even signal.

point, i.e., a bifurcation to or from the trivial solution $p_n = 0$. For the map defined by Equation (13), there are two such bifurcation points, at $\gamma = 4$ and $\gamma = 6.5433$ (see Figure 3(B)).

The intermittency characterizing the sequence plotted in Figure 5 is *not* on-off intermittency, at least not in the strict sense implied by Platt, Spiegel, and Tresser (1993) and Heagy, Platt, and Hammel (1994). The adopted range of γ_n ($\in [4.5, 6.5]$), while covering most of the γ range characterized by non-trivial behavior, is too small to push the system past the critical bifurcations at $\gamma = 4$ and $\gamma = 6.5433$. What is happening instead is that the fluctuations are at times pushing the solution outside the basin of attraction of the attractor, i.e., outside the dashed closed contour in Figure 3(B). A typical 'onset' to a quiescent phase is shown in Figure 6(A), in the form of the path in the $\{\gamma_n, p_n\}$ plane followed by the amplitude iterates. Onset begins when a γ fluctuation pushes the iterate far into the chaotic regime (iteration 1354). The map produces a p_{n+1} value near the top of the range, while the next γ_n happens to pull the iterate back into the fixed point regime (iteration 1355), but outside of the attraction basin of the attractor. The next p_n generated by the map is close to the trivial solution (iteration 1356), and, more importantly, at an amplitude value below the lowest extent of the attractor's basin of attraction. From this point on, subsequent fluctuations in γ_n cannot carry the

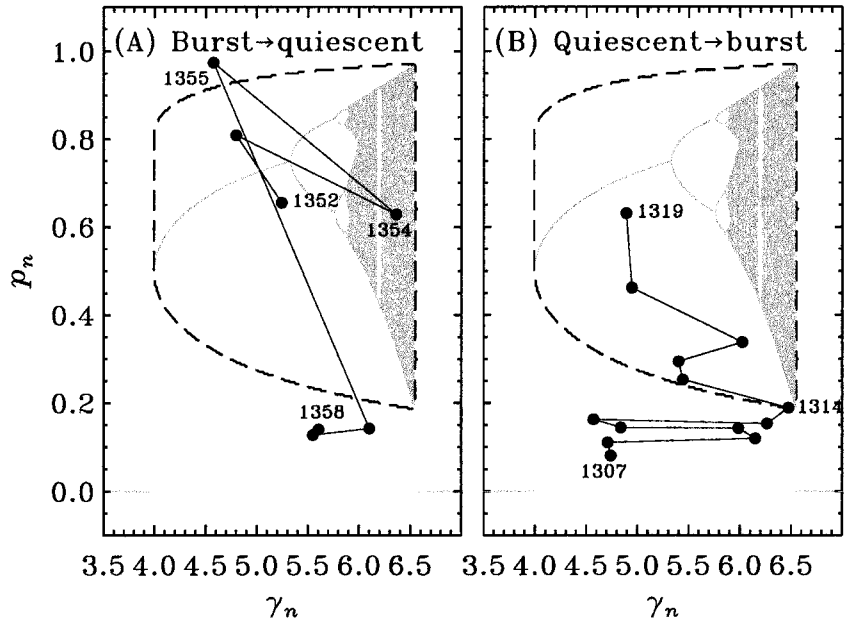

Figure 6. Typical (A) onset, and (B) termination of quiescent phases for the stochastically forced sequence of Figure 5. The *dashed contour* encloses the attraction basin of the attractor.

iterate back towards the attractor. Evidently, this turning-off process can take place in the absence of low-amplitude additive noise.

Once in the attraction basin of the trivial solution, the action of the map is such that $p_{n+1}/p_n < 1$ for any values of γ_n , with the additive noise ε_n in Equation (14) the only mechanism available to keep the iterates $p_n \sim \varepsilon_n$, away from $p_n = 0$.

The end of a quiescent phase (Figure 6(B)) comes about when the distorted random walk – loosely speaking – associated with the cumulative effect of the low-amplitude additive noise takes the iterate near the low point of the basin boundary (iterations 1307 to 1314 on Figure 6(B)). Once the boundary is crossed, the iterate is then pulled back up towards the attractor, corresponding to the onset of a new bursting phase (iterations 1314 $\rightarrow$ 1319). Unlike with the onset of the quiescent phase, the presence of low-amplitude additive noise is now crucial. There exists a threshold value for ε above which this happens in a finite time. For the γ range considered here, this threshold value is $\varepsilon^* \simeq 0.065$, based on a (small) set of 10^8 iteration Monte Carlo runs.

The average waiting time $\langle \Delta\tau \rangle$ between successive bursts increases rapidly as one approaches ε^* from above: $\langle \Delta\tau \rangle = 48$ iterations at $\varepsilon = 0.09$, up to 180, 8850, and 89400 for $\varepsilon = 0.08$, 0.07, and 0.067, respectively. Something like this was to be expected, since $\langle \Delta\tau \rangle \rightarrow \infty$ as $\varepsilon \rightarrow \varepsilon^*$, by definition of the intermittency threshold.

In term of Babcock–Leighton models of the solar cycle, one might conjecture that bursting phases correspond to epochs where the toroidal fields strength in the shear layer is high enough for toroidal flux ropes to form and rise coherently to the surface. Quiescent phases could either be due to the toroidal magnetic fields being so strong that active regions emerge without the E–W tilt necessary to the Babcock–Leighton mechanism, or too weak for flux ropes to lose stability and/or rise coherently to the surface. In the former case the onset of the subsequent 'normal' bursting phase occurs once resistive dissipation has sufficiently decreased the toroidal field strength in the shear layer. In the latter case magnetic field injected from the convection zone is required to restart the dynamo. This is the kind of process embodied by the additive noise ε_n in Equation (14), and seems to be a robust mechanism to restart a dynamo with a lower operating threshold (see Schmitt, Schüssler, and Ferriz-Mas, 1996, for another example in the context of a different dynamo model).

3.3. PREDICTABILITY

If one takes at face value the intermittent behavior characterizing the solution plotted in Figure 5, then the quiescent phases are to be identified with prolonged periods of strongly reduced cyclic activity, i.e., Maunder minimum-like epochs. This immediately leads to the following questions: (1) Is there a 'typical' duration to quiescent or bursting phases? (2) Is it possible to predict the onset and/or duration of quiescent phase, or of bursting phases? We consider each question in turn.

The above discussion – and Figure 6 – have already made it clear that the termination of quiescent phases is driven by the imposed additive white noise, while their onset is triggered by the stochastic fluctuations of the map's control parameter γ_n. *A priori*, this does not augur well for predictability! Indeed, scatter plots of burst duration versus duration of the preceding quiescent phase, or of quiescent phase duration versus duration of the preceding bursting phase, show no sign of a correlation, let alone statistically significant ones.

From an iterate sequence similar to Figure 5 but of much longer duration, it is possible to construct frequency distributions $h(\tau)$ for the duration τ of bursting phases, and distribution $h(\Delta\tau)$ of waiting time $\Delta\tau$ from the end of a bursting phase to the onset of the next. An iterate p_n is deemed to belong to a quiescent phase provided $p_n \leq 0.2 + \varepsilon/2$, corresponding to the highest extent of the lower portion of the trivial solution's attraction basin, plus the mean amplitude of the additive noise. Two successive such iterates are needed to define a quiescent phase. Figure 7 shows these two distributions, constructed from a 10^9 iterations run with $\gamma_n \in [4.5, 6.5]$ and $\varepsilon_n = [0, 0.0667]$. This puts the simulation close to the intermittency threshold $\varepsilon^* = 0.065$, while yielding good statistics for a simulation of this length. Both distributions have an exponential form, in contrast to the power law characterizing the frequency distribution of quiescent phase in the forced logistics

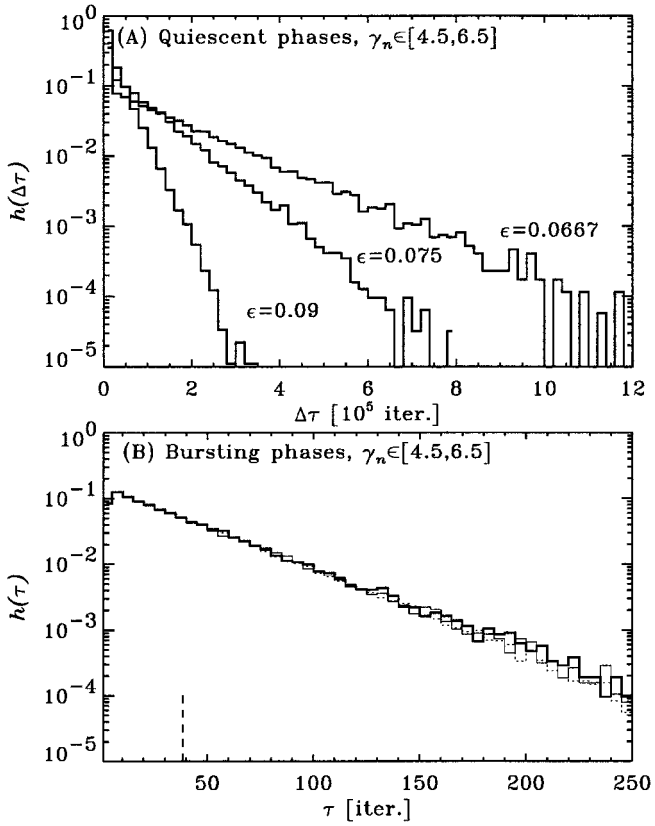

Figure 7. Frequency distributions of quiescent-phase duration $h(\Delta\tau)$ (A) and bursting duration $h(\tau)$ (B), for three stochastically forced sequences with $\gamma_n \in [4.5, 6.5]$ and $\varepsilon = 0.0667$, 0.075 and 0.09 (see Equation (14)), as indicated. The lower threshold demarcating bursting behavior from quiescence is set at $p = 0.2+\varepsilon/2$, corresponding to the upper extent of the trivial solution's attraction basin boundary (see Figure 3(B)), plus the mean value of the additive noise. A minimum of two successive such iterates is needed to define a quiescent phase. The marked excess of very short inter-burst intervals (lowest bin on Figure 7(A)) is associated with the sporadic appearance, within a bursting phase, of 'near misses' quiescent onsets, as at $n = 548$ on Figure 4(A). The $h(\tau)$ distributions (B) for $\varepsilon = 0.075$ and 0.09 (*thin solid* and *dotted* histograms, respectively) are statistically indistinguishable from the $\varepsilon = 0.067$ distribution plotted in (B) as the *solid-line* histogram, and have effectively the same mean, indicated by the *dashed-line* segment along the abscissa.

map near threshold studied by Heagy, Platt, and Hammel (1994). This is yet another indication that the intermittency behavior of Equation (14) is distinct from classical on-off intermittency.

The frequency distribution of quiescent phase duration (Figure 7(A)) steepens as the additive noise amplitude ε is increased beyond the intermittency threshold. On the other hand, the frequency distribution of burst durations (Figure 7(B)) is largely insensitive to the adopted value of ε, provided $\varepsilon \ll 1$. This again confirms that the onset of quiescent phases is triggered by the dynamical properties of the

map, rather than by the additive noise. Even though the burst duration distributions all have the same well-defined mean for ε not too far above threshold, the substantial width of $h(\tau)$ makes this mean of little practical use in predicting the time of return to a quiescent state, once a bursting phase has begun. Moreover, an exponential distribution of event rates is indicative of an underlying Poisson process, implying that each bursting 'event' is indeed fully independent of its predecessors, and so fundamentally unpredictable on the basis of the statistics of former events.

There is one pattern that often announces the onset of a quiescent phase: a pronounced odd–even effect in the amplitude sequence. This is already visible in Figure 4(B) from $n = 540$ to 546, which is immediately followed by a near-miss quiescent phase, as can be seen from the corresponding amplitude drop at $n = 548$ in Figure 4(A). Such a pattern, of varying duration, is actually present prior to 10 out of 12 quiescent phase onsets in Figure 5, as indicated along the upper horizontal axis. The existence of this pattern is readily understood upon recalling that the onset of quiescent phases involves excursions in the chaotic regime of the map, with the entry in the attraction basin of the trivial solution following from an appropriate fluctuation in γ_n (see Figure 6(A)).

4. Comparison with a Numerical Simulation

The results discussed in the preceding section indicate that the odd–even effect is a robust feature of stochastically-forced iterative maps inspired by a dynamo mechanism including a time delay comparable to the cycle period. This being the case, odd–even behavior should then be observed in models of Babcock–Leighton dynamos including stochastic forcing. Charbonneau and Dikpati (2000) have recently presented a series of such simulations. One of these, discussed in Section 3.3 of their paper, shows a spread in cycle periods and anti-correlation between cycle duration and amplitude that both compare favorably to sunspot data. This is a strongly fluctuating model, with 100% fluctuation amplitude in the meridional circulation and 200% fluctuation in the Babcock–Leighton source term. Figure 8(A) shows the corresponding raw and detrended amplitude sequences for the 50 cycles simulated by Charbonneau and Dikpati (2000). The odd–even effect is indeed clearly present for long simulation intervals.

The basic Babcock–Leighton model underlying the Charbonneau and Dikpati (2000) simulations is described in detail in Dikpati and Charbonneau (1999). This axisymmetric, kinematic nonlinear model involves the solution of two coupled partial differential equations governing the evolution of the toroidal field B and poloidal field $\mathbf{B}_p$, which is written in terms of a toroidal vector potential A, so that $\mathbf{B}_p = \nabla \times (A\hat{\mathbf{e}}_\phi)$. Schematically, the governing equations have the form

$$\frac{\partial A}{\partial t} = (\text{Diffusion}) + (\text{Advection}) + s_0 S(r,\theta)\frac{B(r_c,\theta)}{1 + (B(r_c,\theta)/(B_0)^2}\,, \tag{15}$$

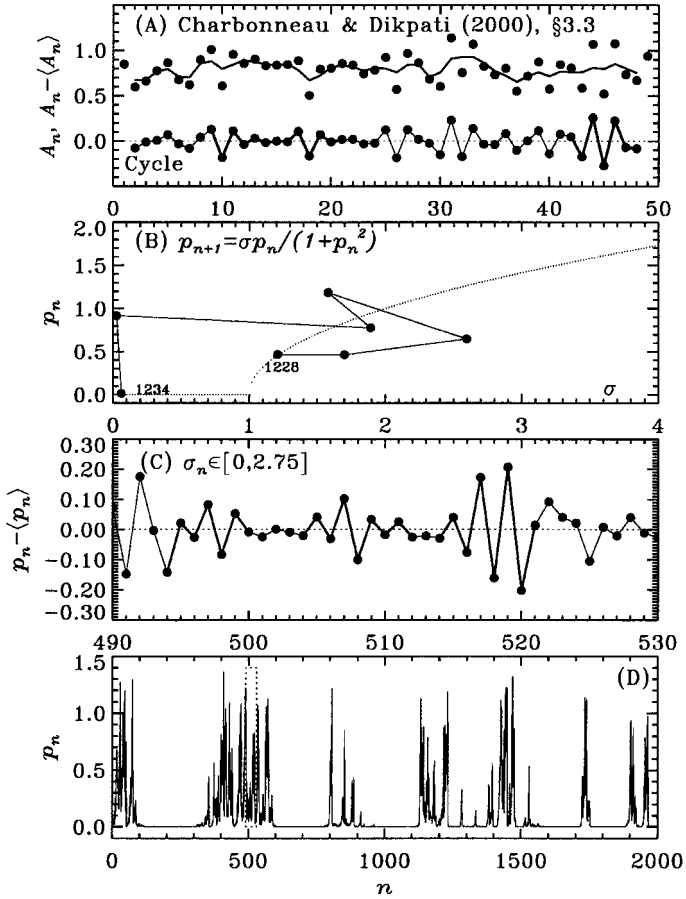

Figure 8. (A) shows the odd–even effect in the raw (*top trace*) and detrended (*lower trace*) amplitude sequences extracted from the stochastically forced Babcock–Leighton dynamo solution discussed in Section 3.3 of Charbonneau and Dikpati (2000). (B) shows the bifurcation diagram for a map derived from the nonlinearity used in that simulation. (C) shows a sequence of amplitude iterates for a stochastically forced version of that map, with $\sigma_n \in [0, 2.75]$. The odd–even effect shows up quite clearly, despite the absence of limit cycles for this map. (D) is a longer iterate sequence, showing that this map exhibits classical on-off intermittency at this level of stochastic forcing.

$$\frac{\partial B}{\partial t} = (\text{Diffusion}) + (\text{Advection}) + r \sin\theta \mathbf{B}_p \cdot \nabla\Omega \,, \tag{16}$$

where the last term on the right-hand side of Equation (15) is a surface source term for the Babcock–Leighton mechanism, which is expressed in terms of the toroidal field B at the core–envelope interface r_c (for further discussion see Section 2.3 of Dikpati and Charbonneau 1999, and Section 2.1 of Charbonneau and Dikpati 2000). With diffusion neglected in the Durney reduction procedure, and with advection subsumed in the time delay, the correspondence between Equations (15) and (9) requires that one sets

$$f(t_{n+1};\sigma) = (\bar{P}/\bar{T})\sigma(1+t_{n+1}^2)^{-1}\,, \quad \sigma > 0 \tag{17}$$

in Equation (6), yielding the map:

$$p_{n+1} = \sigma p_n(1+p_n^2)^{-1}\,, \quad [\ \equiv g(p_n;\sigma)\ ]\,, \quad \sigma > 0\,. \tag{18}$$

Figure 8(B) shows the bifurcation diagram for this map (small dots). It is strikingly different from those plotted in Figure 3. The fixed point $\mu = (\sigma-1)^{1/2}$ emerging from the transcritical bifurcation at $\sigma = 1$ never loses stability to a period-2 limit cycle, as one can easily verify upon evaluating

$$\left.\frac{\mathrm{d}g(p_n;\sigma)}{\mathrm{d}p_n}\right|_{p_n=\mu} = \frac{1-\sigma}{\sigma} > -1\,, \quad \forall\sigma > 0\,. \tag{19}$$

The cascade to chaos through ever higher-order limit cycles that characterized the other maps considered above thus never takes place here. In fact, the non-fluctuating reference simulation of Dikpati and Charbonneau (1999, Section 5) shows a steady cycle amplitude as the source term parameter s_0 is varied over almost two orders of magnitude, suggesting that Figure 8 is indeed a proper – though highly simplified – representation of the solution's dynamical behavior.

Despite the stability of the fixed point solution, a stochastically-forced version of this map exhibits a robust odd–even effect, persisting over many successive iterations, as shown in Figure 8(C). This is a striking result: the odd–even effect does not require a limit cycle, but materializes instead only due to the oscillatory nature of the convergence to the fixed point. The prevalence of an odd–even signal prior to the onset of a quiescent phase is less pronounced than on Figure 5, occurring now seven out of 12 onsets in Figure 8(D).

As with the logistic map studied by Heagy, Platt, and Hammel (1994), the map defined by Equation (18) also exhibits classical on-off intermittency when the control parameter is drawn from a distribution of uniform random deviates $\sigma \in [0, \Sigma]$ straddling the transcritical bifurcation at $\sigma = 1$. Figure 8(D) shows one such intermittent time series, for $\Sigma = 2.75$. The intermittency threshold is found to be $\Sigma^* \simeq 2.69$. The succession of large solid dots in Figure 8(B) shows a typical onset path to a quiescent phase.

5. Discussion and Conclusion

Following a reduction procedure recently proposed by Durney (2000), the behavior of various one-dimensional iterative maps describing the cycle amplitude variations of Babcock–Leighton models of the solar cycle has been studied in some detail. The explanation put forth by Durney (2000) for the observed odd–even effect in sunspot cycle amplitude was found to be robust with respect to the choice of amplitude-limiting nonlinearity, as well as to the presence of stochastic forcing.

Interestingly, numerical experiments carried out with a map inspired from a numerical simulation of a stochastically forced Babcock–Leighton solar cycle model indicate that a robust odd–even effect can still materialize in the absence of limit cycles, due to the generic oscillatory convergence to the fixed points or limit cycles in this class of iterative maps. Strong stochastic forcing was also found to lead to intermittency in two alternate dynamo-inspired maps, and a strong odd–even signal was found to be a good precursor of quiescent phase onset, at least in one of them. It would be interesting to extract reliable cycle amplitude estimates from the Be^{10} record (Beer, Raisbeck, and Yiou, 1991; Beer, Tobias, and Weiss, 1998) immediately prior to the Maunder minimum, to search for an odd–even signal.

Efforts to search for signatures of aperiodicity, chaos and/or intermittency in various types of nonlinear dynamo models have generated a voluminous literature in the past two decades, of which a critical review is well beyond the scope of this paper. Suffices to say that such behaviors do materialize in many classes of solar cycle models of varying degrees of mathematical and/or physical complexity (see, e.g., Weiss, Cattaneo, and Jones, 1984; Schmalz and Stix, 1991; Roald and Thomas, 1997; Tworkowski *et al.*, 1998, and references therein). All but the last of these models essentially rely on the nonlinear dynamical interaction between a small number of degrees of freedom representing field variables, much in the manner originally expounded by Lorenz (1963). The behavior of these models tends to depend rather sensitively on the choice of nonlinearities, and the manner in which the dynamo equations are truncated to a low order dynamical system. In addition, mean-field or mean-field-like dynamo models subjected to stochastic forcing have been found to exhibit significant amplitude modulation (e.g., Ossendrijver and Hoyng, 1996, and references therein) and even something akin to intermittency (Schmitt, Schüssler, and Ferriz-Mas, 1996), but not the odd–even effect, at least as far as one can judge from the published results. The approach followed in this paper uses a model that is in fact simpler that even the more severely truncated of the models cited above, but relies instead on a long time delay ('long' in the sense of being of the order of the cycle period) to generate complex behavior. Moreover, the complexity is crucially linked to this time delay, while being rather insensitive to the choice of amplitude-limiting nonlinearity.

An essential condition for the reduction of the dynamo equations to a one-dimensional map is thus the existence of a time delay in the dynamo process. Such a time delay arises naturally in models of the Babcock–Leighton type, because of the finite time required for meridional circulation to advect the poloidal field from the surface layers down to the shear layer at the core – envelope interface. In fact, the assumed circulation flow speed turns out to be the primary determinant of the cycle period in such models (see, e.g., Dikpati and Charbonneau, 1999, Section 4). This is after all why, in Equation (3), the production of the toroidal field T_{n+1} is made proportional to the poloidal field P_n from the preceding cycle.

In contrast, in models based on mean-field electrodynamics (e.g., Moffatt, 1978) and where the shear and α-effect coexist spatially, one would have to write some-

thing like $T_n \sim P_n$ and $P_n \sim T_n$, so that reduction to a one-dimensional iterative map is evidently not possible, unless long time delays are artificially introduced in the model, as in the simulations discussed by Yoshimura (1979), for example. One true exception might be the so-called interface dynamos, in cases where the regions of shear and α-effect are spatially segregated, as considered for example by MacGregor and Charbonneau (1997). In such models the two source regions must communicate on a time scale of the order of the diffusion time based on their spatial separation, which then sets the cycle period. At this writing the effects of stochastic forcing on such models remain undocumented.

Acknowledgements

I wish to thank Bernard Durney for sending me a copy of his 'odd–even' paper prior to publication, and James Norman for bringing to my attention the Heagy, Platt, and Hammel (1994) paper. Thanks are also due to Mausumi Dikpati for providing the numerical data for Figure 8(A), and to Mark Rast, Bernard Durney, and the referee, Peter Hoyng, for a critical reading of an earlier draft of the paper. The National Center for Atmospheric Research is sponsored by the National Science Foundation.

References

Beer, J., Raisbeck, G. M., and Yiou, F.: 1991, in C. P. Sonett, M. S. Giampapa, and M. S. Matthews (eds.), *The Sun in Time*, p. 343
Beer, J., Tobias, S., and Weiss, N.: 1998, *Solar Phys.* **181**, 237.
Caligari, P., Moreno-Insertis, F., and Schüssler, M.: 1995, *Astrophys. J.* **441**, 886.
Charbonneau, P. and Dikpati, M.: 2000, *Astrophys. J.* **543**, 1027.
Dikpati, M. and Charbonneau, P.: 1999, *Astrophys. J.* **518**, 508.
D'Silva, S. and Choudhuri, A.R.: 1993, *Astron. Astrophys.* **272**, 621.
Durney, B. R.: 1997, *Astrophys. J.* **486**, 1065.
Durney, B. R.: 2000, *Solar Phys.* **196**, 421.
Feigenbaum, M. J.: 1978, *J. Stat. Phys.* **19**, 25.
Heagy, J. F., Platt, N., and Hammel, S. M.: 1994, *Phys. Rev. E* **49**, 1140.
Holton, D., and May, R. M.: 1993, in T. Mullin (ed.), *Chaos and One-Dimensional Maps, The Nature of Chaos*, Oxford University Press, Oxford, p. 69.
Hoyng, P.: 1993, *Astron. Astrophys.* **272**, 321.
Hoyt, D. V. and Schatten, K. H.: 1998, *Solar Phys.* **181**, 491.
Longcope, D. W. and Fisher, G. H.: 1996, *Astrophys. J.* **458**, 380.
Lorenz, E. N.: 1963, *J. Atmospheric Sci.* **20**, 130.
MacGregor, K. B. and Charbonneau, P.: 1997, *Astrophys. J.* **486**, 484.
Moffatt, H. K.: 1978, *Magnetic Field Generation in Electrically Conducting Fluids*, Cambridge University Press, Cambridge.
Moreno-Insertis, F., Caligari, P., and Schüssler, M.: 1995, *Astrophys. J.* **452**, 894.
Nandy, D. and Choudhuri, A. R.: 2000, preprint.
Ossendrijver, A. J. H. and Hoyng, P.: 1996, *Astron. Astrophys.* **313**, 959.

Ossendrijver, A. J. H., Hoyng, P., and Schmitt, D.: 1996, *Astron. Astrophys.* **313**, 938.
Platt, N., Spiegel, E. A., and Tresser, C.: 1993, *Phys. Rev. Letters* **70**, 279.
Roald, C. B. and Thomas, J. H.: 1997, *Monthly Notices Royal Astron. Soc.* **288**, 551.
Schmalz, S. and Stix, M.: 1991, *Astron. Astrophys.* **245**, 661.
Schmitt, D., Schüssler, M., and Ferriz-Mas, A.: 1996, *Astron. Astrophys.* **311**, L1.
Tworkowski, A., Tavakol, R., Brandenburg, A., Brooke, J. M., Moss, D., and Tuominen, I.: 1998, *Monthly Notices Royal Astron. Soc.* **296**, 287.
Weiss, N. O., Cattaneo, F., and Jones, C. A.: 1984, *Geophys. Astrophys. Fluid Dyn.* **30**, 305.
Wilson, R. M.: 1988, *Solar Phys.* **117**, 269.
Yoshimura, H.: 1979, *Astrophys. J.* **227**, 1047.